



OPEN

Low-profile conformal single-sided miniaturized frequency selective surface for wideband shielding

Malathi Kanagasabai¹, Lavanya Viswanathan¹, M. Gulam Nabi Alsath¹,
 Sandeep Kumar Palaniswamy²✉, Sachin Kumar³, Santhya Premdharsini Premkumar¹,
 Hyun Chul Choi⁴ & Kang Wook Kim⁴✉

This paper presents an ultra-wideband (UWB) frequency selective surface (FSS) that is conformal, low-profile, single-layered, and miniaturized. The designed simple modified star swastika (MSS) arms offer a wide bandwidth of 7.5 GHz with transmission nulls ranging from 3.1 to 10.6 GHz. The $0.0008\lambda_0$ thin MSS FSS unit cells form a periodic pattern with a physical form factor of $0.041\lambda_0$ and 61% miniaturization. The proposed FSS has a -10 dB fractional bandwidth of 109.48% and a peak shielding of 67.9 dB at 7.1 GHz. The designed FSS has a figure of merit (FoM) of 10.25 (λ_0/U), where U represents the unit cell size of the FSS. In both transverse electric (TE) and transverse magnetic (TM) modes, incoming waves can be stable with incidence angles (θ) up to 75° and less than 1% frequency deviation. To gain a physical understanding of the FSS unit cell, an equivalent circuit model (ECM) analysis is conducted. The FSS prototype has been built, and the measured results are validated with simulated results. Hence, the proposed MSS FSS could be a promising solution for wideband shielding.

Wireless communication in the modern world has changed the way people interact, communicate, and access information, providing portability, ease, scalability, and flexibility^{1,2}. A wideband spectrum is used in hospitals, smart homes, and smart environments due to its extensive coverage^{3,4}. However, mutual interference in the ultra-wideband (UWB) spectrum caused by nearby users does not provide better spectrum management, direct wireless signal, or data security^{5,6}. The frequency selective surface (FSS) is made up of an array of subwavelength-sized metallic patches or grids printed on a dielectric substrate to reduce interference^{7,8}. In many cases, the UWB FSS can be combined with the UWB antenna to increase its gain⁹. Designing an FSS on a single-layer, single-sided substrate with a small footprint to prevent UWB without changing the polarisation and angular stability for an incoming wave of ϕ and θ is challenging.

Recently, several wideband FSS structures have been designed in^{10–31}. In order to achieve a miniaturized size, 2.5D FSS with vias connecting the top and bottom layers is reported in^{10–12}. The FSS is constructed in a 2D framework to reduce cost and make fabrication easier. Multilayer arrangements with multiple substrate and conductive layers are reported in^{13–17,29}. A mesh grid with a dimension of $0.07\lambda_0$ is sandwiched between a square loop with interdigitated bends¹³. A circular loop is embedded on the top and bottom layers in¹⁴, while a square grid is developed in the centre layer to achieve miniaturization of $0.07\lambda_0$.

A stacked FSS structure with parallel strip lines with a size of $0.07\lambda_0$ is presented in¹⁵. In¹⁶, incorporating three conductive layers with square and cross-parasitic patches on two dielectric substrates with a unit cell size of $0.093\lambda_0$ can reject frequencies between 3.49 GHz and 12.13 GHz. Even though multi-layer FSS provide more bandwidth, they make the profile bulkier, therefore a single-layer FSS is created. A combined swastika-shaped and circular loop¹⁷, cross-shaped convoluted arms¹⁸, and a cross pattern enclosed in a circle¹⁹ are etched on the top and bottom layers of the substrate, resulting in a relatively larger profile thickness. In²⁰, a wide band-stop FSS is designed using a modified Greek cross fractal element. The fractal technique offers a higher bandwidth of 13.69 GHz and a wider profile of $0.2\lambda_0$. The band-stop FSS at 3.5 GHz is designed using the interdigital topology, which has a larger footprint of $0.1\lambda_0$ ³². Furthermore, the wide band-stop FSS in^{20,23–25,33,35} uses the FR4 substrate, making the structure unsuitable for conformal applications. The technique reported for wideband shielding in^{34,38} has a miniaturized form factor, the operating frequency is limited to 2 GHz and 3.5 GHz, respectively.

¹Department of Electronics and Communication Engineering, College of Engineering, Guindy, Anna University, Chennai 600025, India. ²Department of Electronics and Communication Engineering, Faculty of Engineering and Technology, SRM Institute of Science and Technology, Kattankulathur 603203, India. ³Department of Electronics and Communication Engineering, Galgotias College of Engineering and Technology, Greater Noida 201310, India. ⁴School of Electronic and Electrical Engineering, Kyungpook National University, Daegu 41566, Republic of Korea. ✉email: vrpchs@gmail.com; kang_kim@ee.knu.ac.kr

The angular stability of the FSS refers to its ability to generate a stable frequency response for incoming theta (θ) electromagnetic waves. Polarization insensitivity indicates that the band-stop response remains constant regardless of the incident EM waves' angles of phi (φ). In electromagnetic mitigation, where the FSS is mounted on the room's walls, higher angular stability and polarization insensitivity are preferred, allowing the FSS to produce a stable frequency response when electromagnetic waves arrive from different directions with different polarization states. In addition to a lack of structural specifications, the two-fold symmetrical geometry of FSS prevents it from providing high angular stability^{17,18,21,28,36,37} and polarization insensitivity²⁷. In the above-mentioned literature, some major issues are the larger size of the FSS unit cell, lack of polarization-insensitivity and conformability, low angular stability, multi-layer configuration, and the high profile of the FSS.

This paper presents a simple low-cost technique for obtaining single-layer, single-sided miniaturized FSS to address the aforementioned issues. The presented FSS has a periodicity of $0.041\lambda_0$ and is embedded on the top layer of the flexible polyester substrate. The proposed FSS has a UWB band stop response from 3.1 GHz to 10.6 GHz, with angular stability up to 75°. Its symmetric structure is polarization-insensitive for both TE and TM modes.

Design of the FSS unit cell

Design procedure

In Fig. 1a, a perfect electric conductor (PEC) of (h) 35 μm is printed on a flexible polyester substrate of (t) 50 μm with dimensions of 4 mm \times 4 mm. The substrate, with a low dielectric constant and loss tangent (K) of 2.8 and 0.0045, respectively, helps to increase bandwidth, thereby improving FSS performance. The FSS is formed using the stepped impedance technique, which consists of metallic arms and slots with varying lengths and widths. A modified star slot is added between the simple swastika arm to limit its width, reducing the coupling effect and achieving the wide bandwidth. The modified star swastika (MSS) FSS unit cell has a miniaturised footprint of $0.041\lambda_0 \times 0.041\lambda_0$, where λ_0 represents the lowest operating frequency. The side view of the proposed FSS unit cell is depicted in Fig. 1b. When electromagnetic waves with frequencies ranging from 3.1 GHz to 10.6 GHz are incident on the proposed FSS unit cell, they are reflected as shown in Fig. 1c. At resonance, the inductance and capacitance as indicated in the equivalent circuit model become short-circuited, resulting in the rejection of the incident waves.

Transition of transmission coefficients at different stages

Figure 2a depicts the design process, which includes the step-by-step construction of metallic strips on a flexible polyester substrate. The first step is to add a PEC to a $0.041\lambda_0$ substrate. In Stage I, an L-Slot with a width (U_1) of 0.3 mm is etched within the unit cell, resulting a band stop response ranging from 5.7 GHz to 13.05 GHz, as shown in Fig. 2b. The band stop response has a significant fractional bandwidth of 78.4%, with the resonant frequency centred at 8.9 GHz.

In Stage II, a modified star-shaped slot made up of two modified square slots is etched in the center of the substrate to achieve an operating frequency of 3.9 GHz to 11.1 GHz with a fractional bandwidth of 96% and good impedance match. Stage III aims to achieve a fractional bandwidth of 109.4% and frequency coverage from 3.1 GHz to 10.6 GHz, with attenuation below -10 dB using a modified L-slot.

Behaviour of surface current pattern and ECM analysis

The MSS FSS is analyzed using the surface current distribution in TE and TM modes at 3.1 GHz and 10.6 GHz, as shown in Fig. 3. The largest width (U_4) of the modified swastika arm allows the MSS FSS to achieve a wide bandwidth. The slot width (U_1) of 0.3 mm, which has a capacitive effect, helps to minimize coupling between adjacent metallic arms. The strong flow of current between L-slots results in the highest operating frequency of 10.6 GHz. The strong current distributed along the swastika arm offers 3.1 GHz in both TE and TM modes.

Theoretically, the total electrical length for the lowest operating frequency is obtained as,

$$L = \frac{C}{4f\sqrt{\frac{\epsilon_r + 1}{2}}} \quad (1)$$

Practically, the total length of the metallic strip is calculated as $L = U_1 + U_2 + U_3 + U_4 + U_5 + U_6 + U_7 + U_8 + V_1 = 16.953$ mm. By substituting, the operating frequency is obtained as 3.2 GHz, which corresponds to 3.1 GHz. The following formula can be used to calculate the bandwidth (BW),

$$BW = \frac{K}{W} \quad (2)$$

where K (= 0.0045) is the material property of the substrate and W is the width of the metallic resonator. Using Eq. (2), the bandwidth is calculated as 7.48 GHz, which is approximately 7.5 GHz. The equivalent circuit model (ECM) using Advanced Design System (ADS) software is illustrated in Fig. 4a.

The inductor (L) and capacitor (C_1) are connected in series to create an effective short circuit configuration, forming transmission nulls with term 1 and term 2 set to 377 Ω . The dielectric substrate is modelled as a transmission line with an impedance of Z_d and height (t). The inductance (L) determines the electrical length of the metallic resonance, whereas the capacitances (C_1, C_2) define the gap (U_1, U_2) between adjacent metallic resonators. The addition of capacitor C_2 in parallel with the series combination results in a wide bandwidth at the resonating frequency of 7.1 GHz. The total impedance of the ECM circuit is calculated and shown in Fig. 4a.

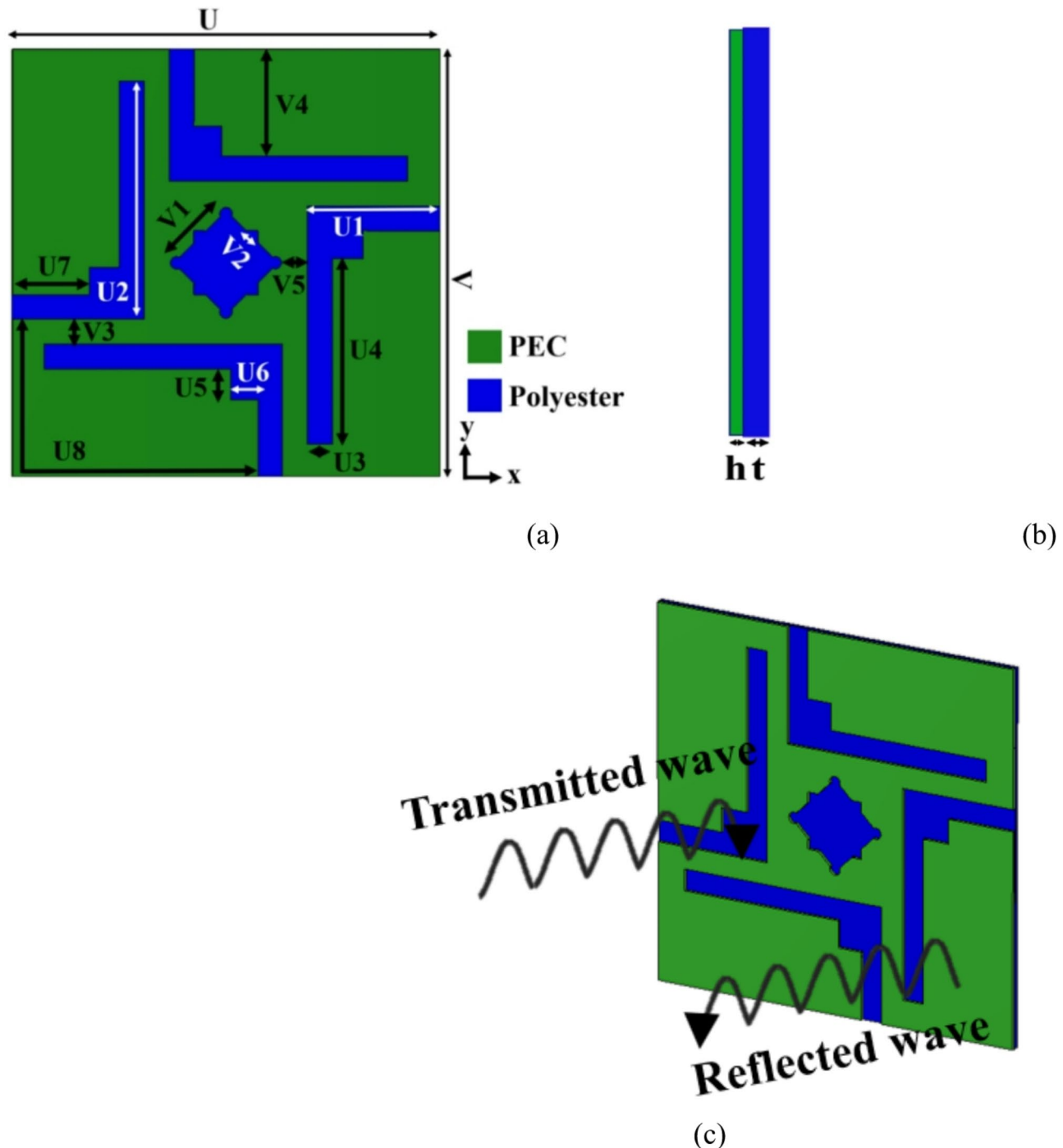


Fig. 1. (a) Design of the proposed FSS unit cell ($U=4$ mm, $U1=2.23$ mm, $U2=3.23$ mm, $U3=0.43$ mm, $U4=2.54$ mm, $U5=0.885$ mm, $U6=0.4$ mm, $U7=1.74$ mm, $U8=4.764$ mm, $V=4$ mm, $V1=0.734$ mm, $V2=0.49$ mm, $V3=0.734$ mm, $V4=1.8$ mm, $V5=0.254$ mm, (b) Side view, (c) Behaviour of incident electromagnetic waves on the proposed band-stop FSS.

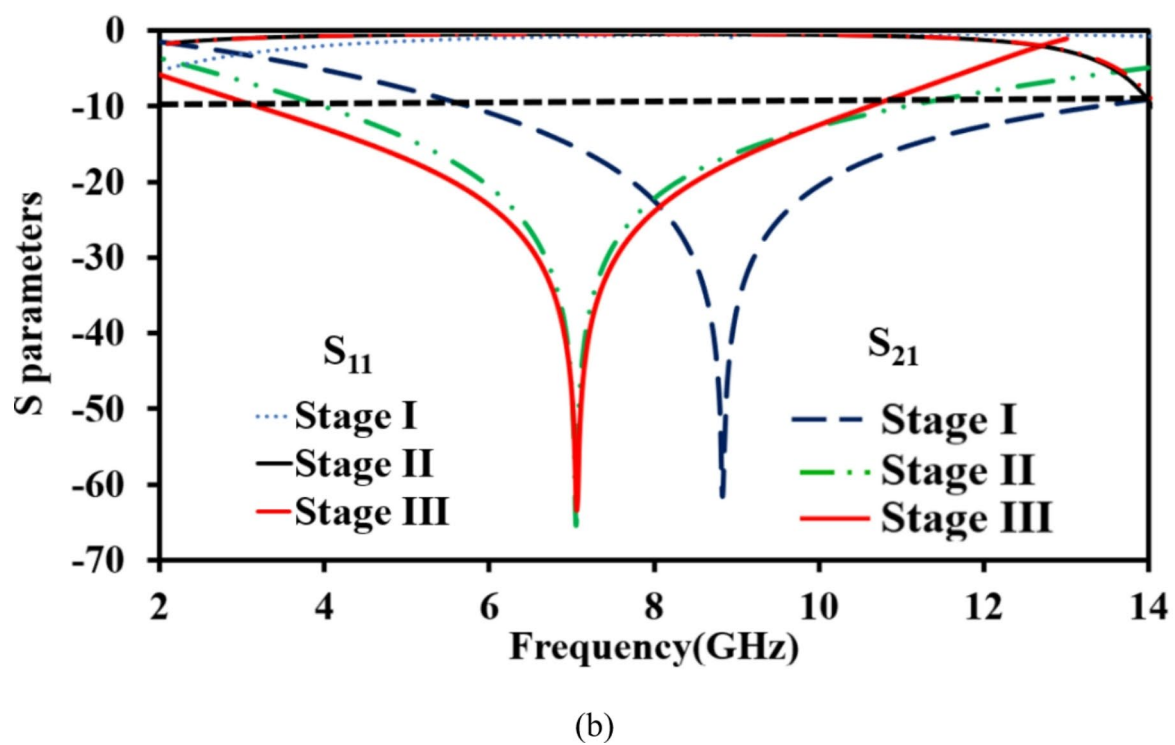
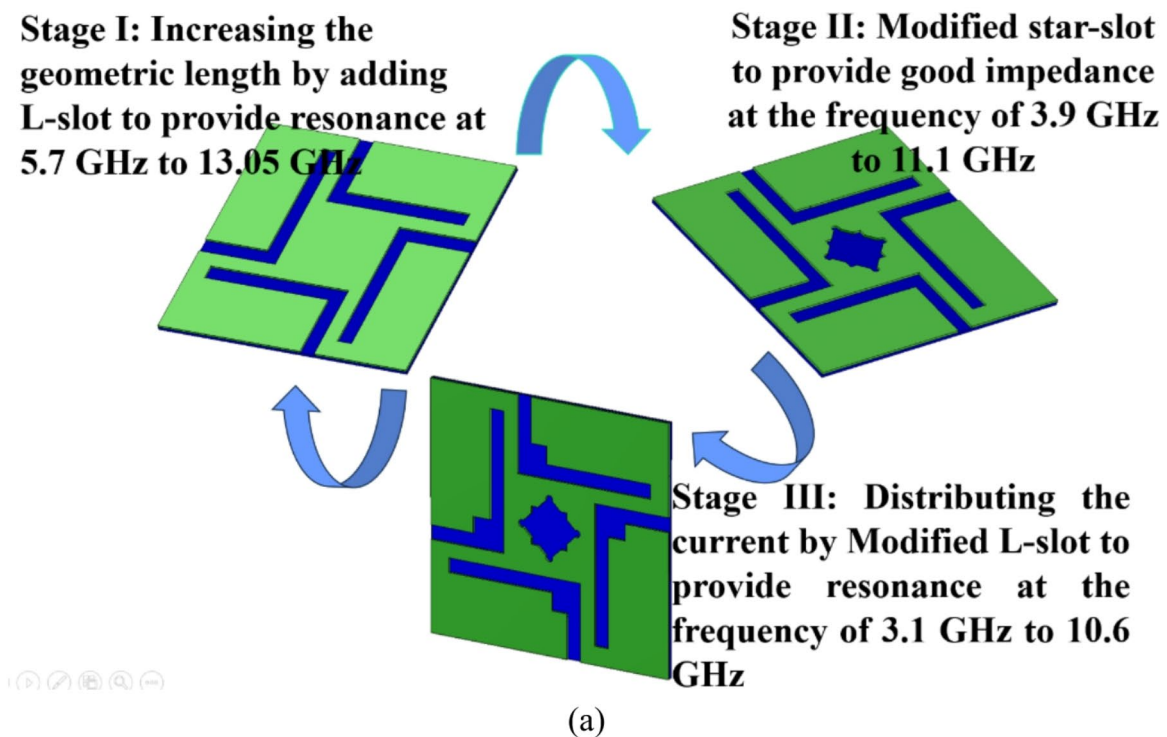


Fig. 2. (a) Evolution stages of the FSS unit cell, (b) S-parameters at each evolution stage.

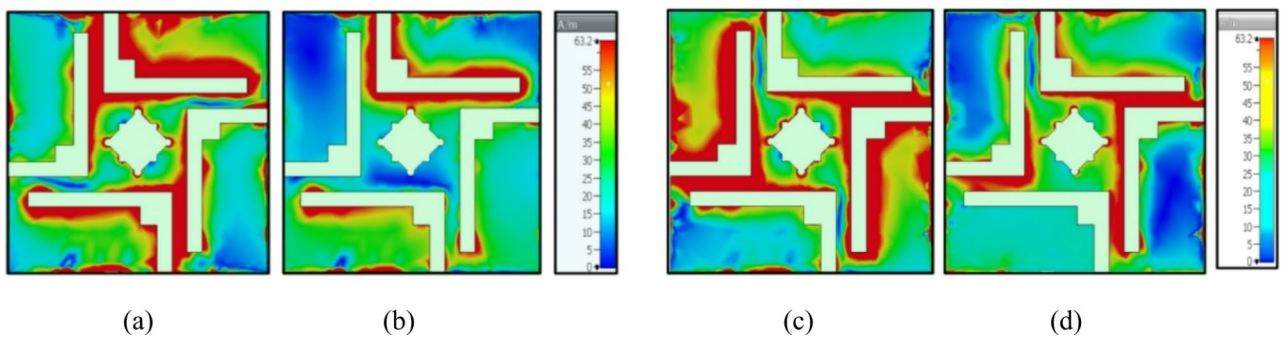


Fig. 3. (a) Surface current distribution on the resonator in TE mode at 3.1 GHz, (b) Surface current distribution on the resonator in TE mode at 10.6 GHz, (c) Surface current distribution on the resonator in TM mode at 3.1 GHz (d) Surface current distribution on the resonator in TM mode at 10.6 GHz.

$$Z = \frac{\left(j\omega L + \frac{1}{j\omega C1}\right) \times \left(\frac{1}{j\omega C2}\right)}{j\omega L + \frac{1}{j\omega C1} + \frac{1}{j\omega C2}} \quad (3)$$

By solving Eq. (4) and equating the transmission poles and zeroes,

$$\omega^2 = \frac{1}{C1L} \quad (4)$$

$$C2 = \frac{C1}{\omega^2 LC1 - 1} \quad (5)$$

The values of L , $C1$, and $C2$ are calculated using Eqs. (5) and (6). The ECM circuit provides an effective band-stop response for the UWB spectrum, covering frequencies ranging from 3.1 GHz to 10.6 GHz, with attenuation levels below -10 dB, as shown in Fig. 4b. To verify the practical simulation values, the operating frequency is calculated using Eq. (6) as,

$$f = \frac{1}{2\pi \sqrt{LC_{eq}}} \quad (6)$$

where $C_{eq} = C1 + C2$. By substituting the values for L , $C1$, and $C2$, the frequency (f) is evaluated as 7.04 GHz (using Eq. (3)), which represents the peak shielding of the band-stop response²⁹.

Parametric analysis

The parametric analysis begins by increasing the width of the conducting arms ($U4$), and results in a significantly wide bandwidth, as shown in Fig. 5. Initially, the width of the conducting arm is set to 0.42 mm, resulting in a bandwidth of 6.134 GHz. In order to increase the bandwidth even further, the width of the P-shaped conducting arm is increased by 0.3 mm, resulting in a broadening of the bandwidth to 6.7 GHz.

An additional 0.3 mm addition in metallic arm width allows for rejection of an even wider band from 3.1 GHz to 10.6 GHz with a bandwidth of 7.5 GHz. Consequently, fractional bandwidth increases to 99.46%, 103.87%, and 109.48% at each stage. The direct relationship between the width of the metallic arms and bandwidth indicates that increasing the arm width ($U4$) naturally contributes to a significant increase in bandwidth range.

Results and discussion

In an experimental prototype, a periodic array of 51×58 elements made of a perfect electric conductor (PEC) is embedded in a 50 μm thick polyester with dimensions of 25.4 cm \times 22.3 cm. The MSS FSS prototype is positioned between two identical horn antennas that are one meter apart. The experiment is carried out in an anechoic chamber with a vector network analyser (N9951A), as shown in Fig. 6, to evaluate the fabricated FSS performance in terms of transmission properties. The angular stability is measured by changing the incident angle of electromagnetic waves by precisely rotating the transmitting antenna from 0° to 75° . Figure 7 depicts the simulated and fabricated S-parameters of the FSS. Simulations were performed with a cylindrical bending radius (R) of 35 mm along the x and y axes to evaluate the conformal nature of the MSS FSS²⁶. The bending radius that produces the bending angle (θ) in degrees is obtained through the radius (R) and length of the array ($L_a = 51(U)$) as⁴⁵

$$\theta \text{ (deg)} = \frac{180^*L_a}{\pi^*R} \quad (7)$$

Notably, the performance of the FSS remains consistent with minimum shift regardless of the bending direction, demonstrating its remarkable ability in conformal applications. The shielding effectiveness (SE) of an FSS refers

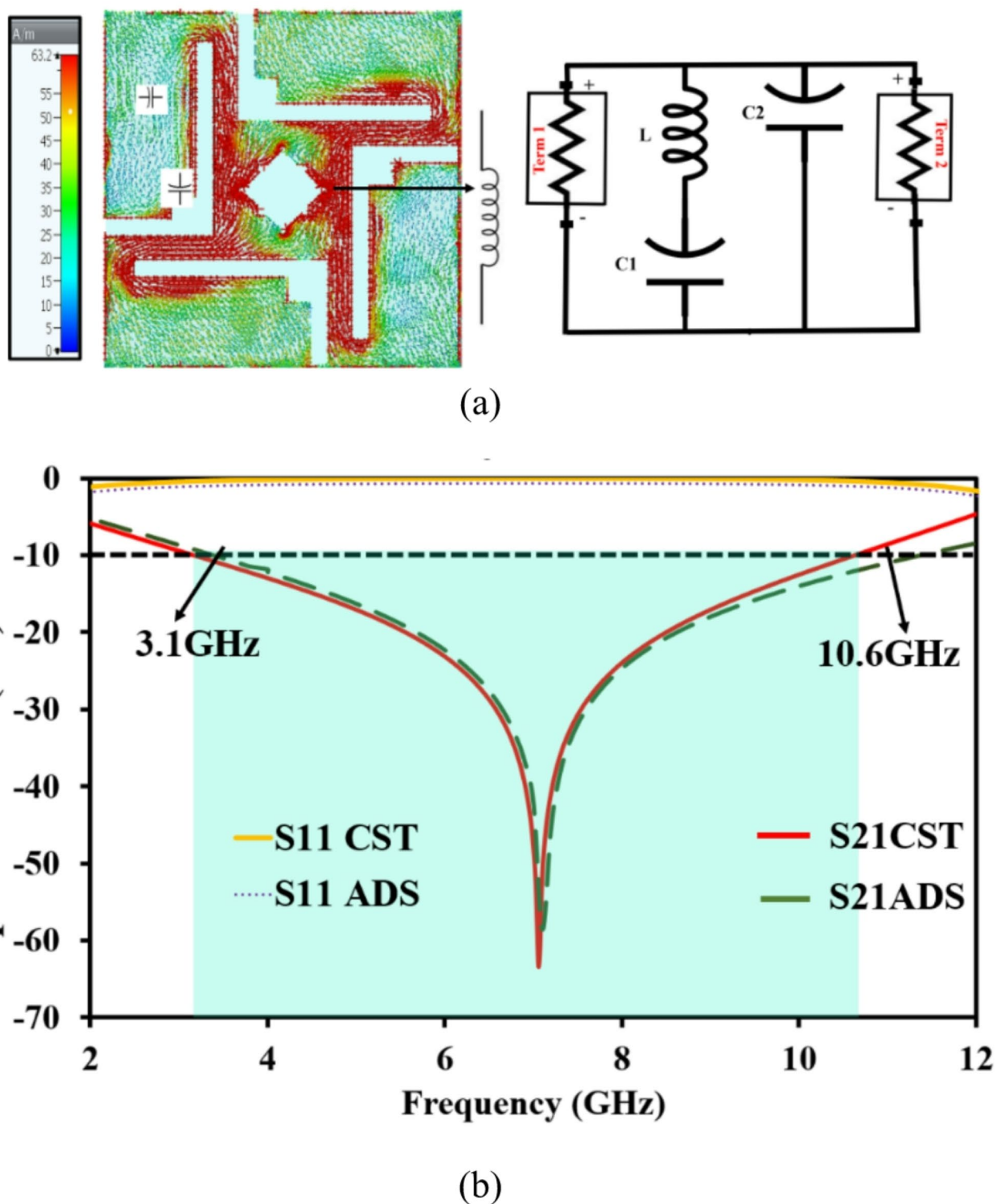


Fig. 4. (a) Circuit model, (b) Simulated $|S_{21}|$ from ADS and CST ($L = 1$ nH, $C1 = 0.23$ pF, $C2 = 0.28$ pF).

to its ability to block specific frequencies of electromagnetic waves while allowing others through. The shielding effectiveness²⁵ is computed between the incident (E_i) and transmitted (E_t) electric fields as,

$$SE (dB) = -20 \left(\frac{E_t}{E_i} \right) \quad (8)$$

The frequency response under different incident angles (θ) and physical form factor (U) is given by²⁴.

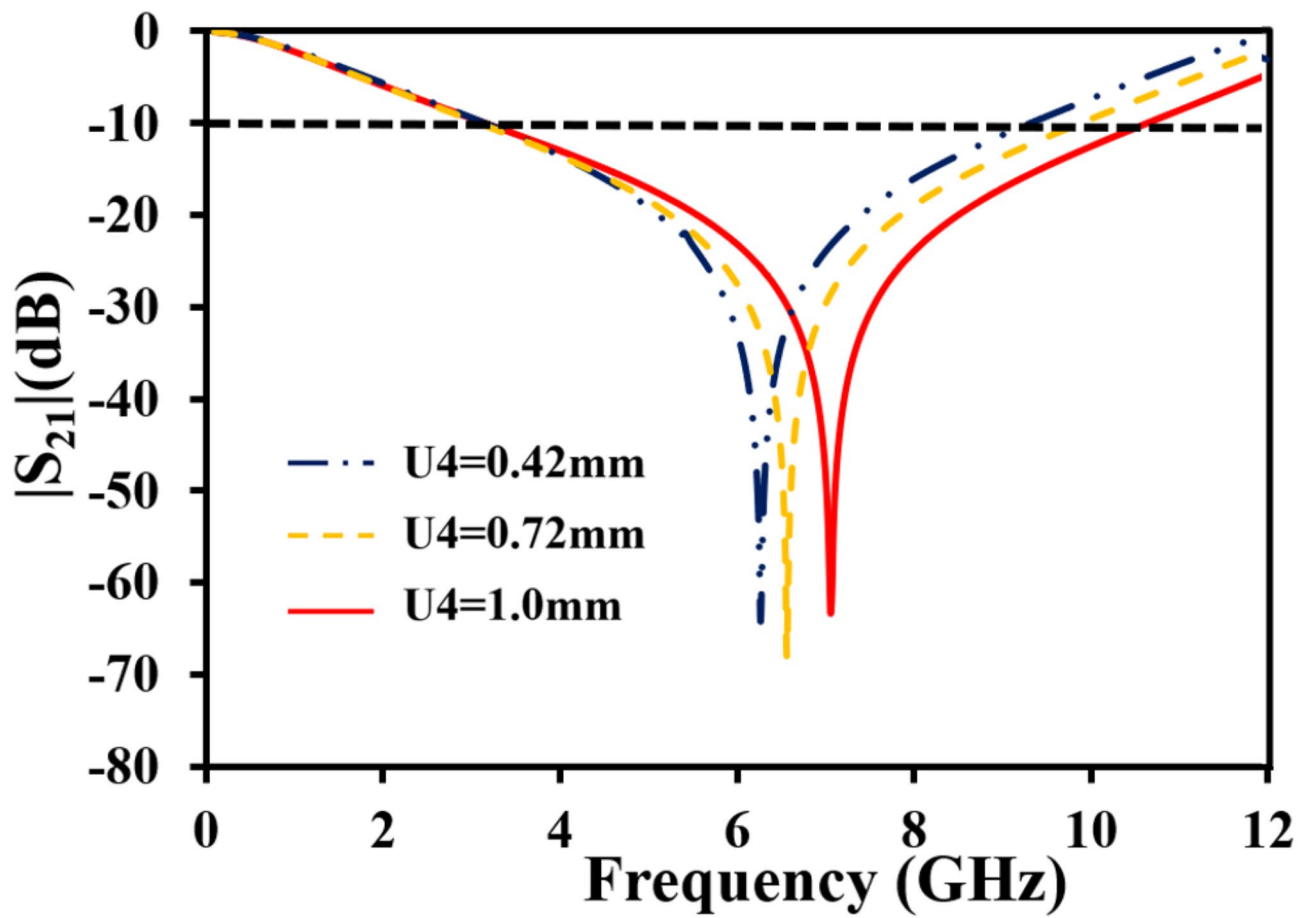


Fig. 5. Parametric analysis for different widths of metallic resonators.

$$U < \frac{\lambda_0}{1 + \sin\theta} \quad (9)$$

For a resonating frequency of 7.1 GHz, the FSS size is calculated to be 21.11 mm with a maximum incident angle of 90°. The MSS FSS has a physical form factor of less than 21.475 mm, ensuring stability up to 75° as shown in Fig. 8²⁴. The value of U is constrained by this limitation. These tests demonstrate the ability of the FSS to maintain stable transmission properties across a wide range of incident angles and polarized electromagnetic waves.

Table 1 compares the proposed FSS to similar existing designs. The proposed UWB-shielded FSS unit cell has the following notable features:

- The proposed UWB shielding FSS has a miniaturized physical form factor of $0.041\lambda_0 \times 0.041\lambda_0$ and covers a frequency range of 3.1–10.6 GHz. In comparison to existing literature^{10,16–19,21,24,29}, the designed FSS achieves impressive size reductions of 65%, 80%, 86.1%, 84%, 94%, 61%, and 69.5%, respectively.
- The miniaturized 2D UWB band-stop FSS presented is more cost-effective than¹⁰ due to the absence of a conducting hole.
- The MSS FSS has a lower profile by incorporating the metallic resonator on the top surface of the polyester, while the FSS in^{10,16–18,29} consists of multiple substrate layers (SL) and conductive layers (CL).
- Unlike FSSs in^{18,24} that have rigid substrates, the proposed MSS FSS is embedded on a conformal polyester substrate, covering the entire UWB range for conformal applications.
- The proposed FSS, unlike^{10,16–19,21,29}, maintains angular stability up to 75° due to its miniaturized footprint design.
- Unlike²⁷, the current art provides polarization insensitivity for oblique angles of phi up to 90° due to its fourfold symmetry.
- The proposed FSS unit cell achieves a 10 dB peak shielding of 67.9 dB when compared to^{10,16–18,21,22,24,29}.

Mitigation of interference is critical to maintain reliable performance, as wideband systems operate over a wide frequency spectrum that overlaps with other wireless systems³⁹. In multi-user UWB scenarios, metamaterial-based surfaces can isolate signals from different users by reflecting or absorbing unwanted frequencies in overlapping regions^{40,41}. In the future, the metamaterial-based layers/surfaces could be embedded in antennas to suppress out-of-band interference and improving signal-to-noise ratio (SNR)⁴². Also, metamaterial-based

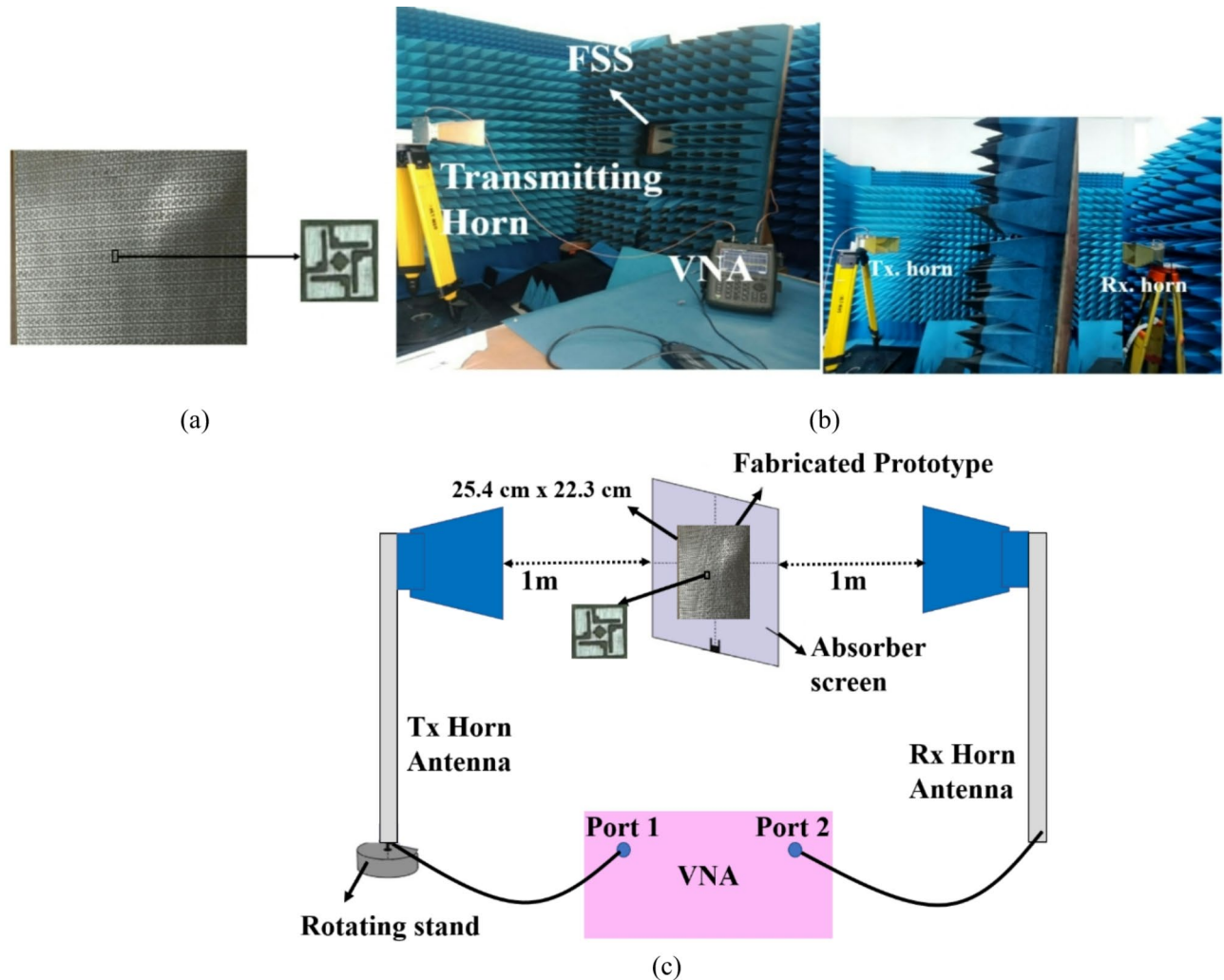


Fig. 6. (a) Fabricated Prototype, (b) Measurement setup, (c) Schematic view of the measurement setup.

panels can be used to shield wideband systems from interference in high-density wireless environments, such as offices or industrial setups^{43,44}.

Conclusion

A single-layer miniaturized FSS designed on a flexible polyester substrate is presented. The FSS has a band-stop response across a large frequency range, effectively spanning from 3.1 to 10.6 GHz, with attenuation below -10 dB. Furthermore, its physical form factor of 4 mm ensures angular stability up to 75° for both TE and TM modes. The agreement between simulated and measured results, combined with bending analysis, further validates the performance of FSS. Hence, the designed FSS could be effectively used in antennas, radomes, and electromagnetic shielding to improve radiation performance by filtering out unwanted signals, selectively allowing certain frequencies for radar systems, or improving shielding in sensitive electronic environments.

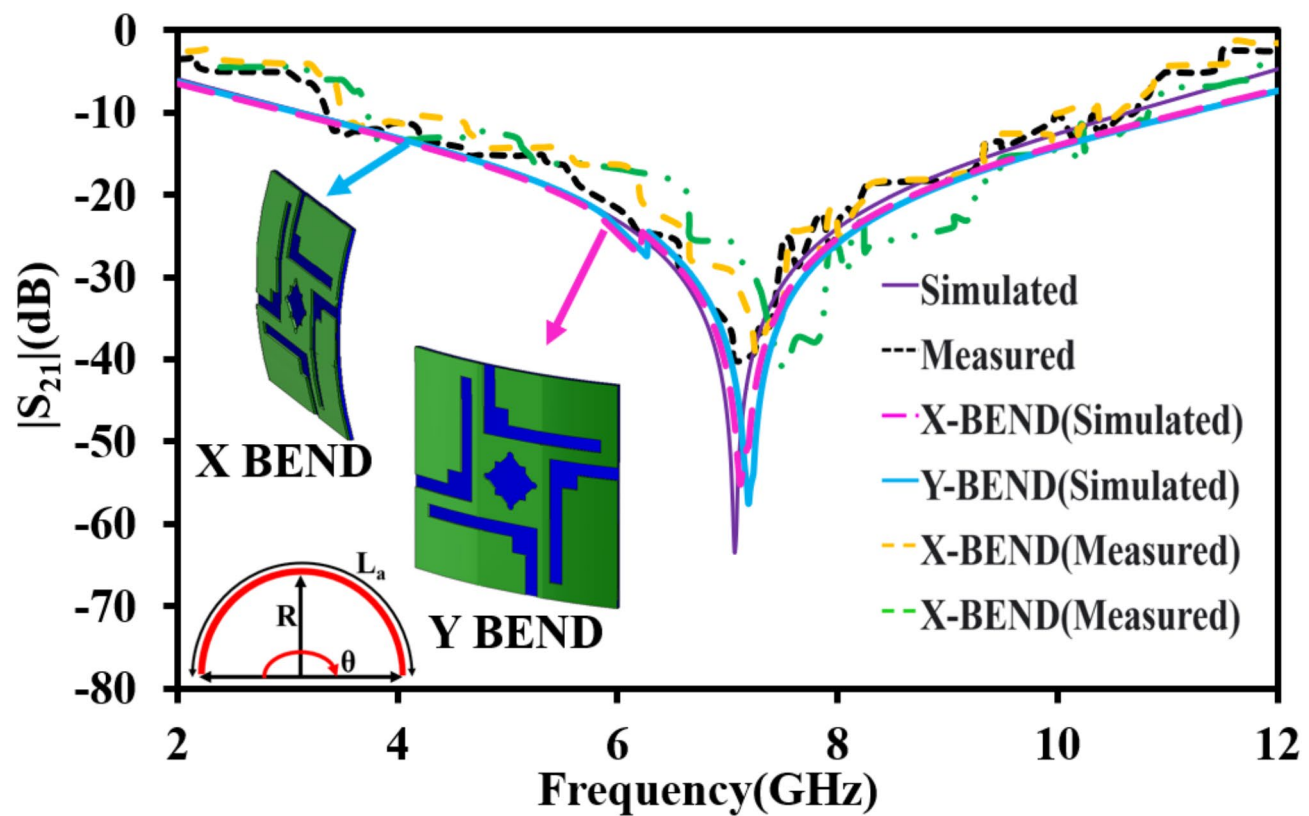


Fig. 7. Comparison of simulated and measured S-parameters with and without bending.

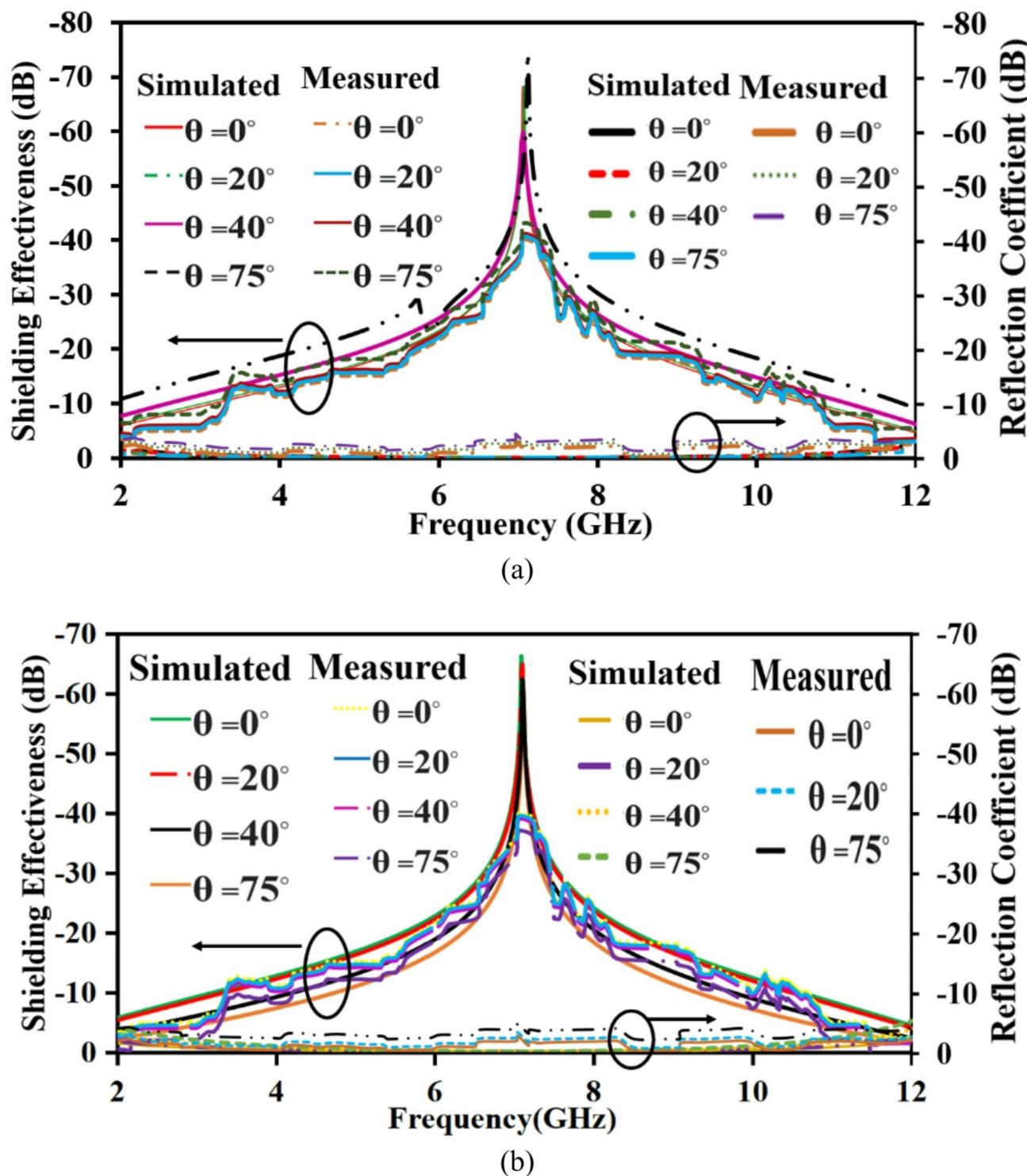


Fig. 8. Comparison of simulated and measured SE for (a) TE polarization, (b) TM polarization.

Ref.	MF (λ_0 , mm ³)	% M	NOR	NOL	OF (GHz)	θ	SE (dB)	S/C	Limitations
10	0.07 $9.6 \times 11.1 \times 0.7$	65	BS	1SL 2CL	1.97–8.08	30°	46*	FR-4/No	Conductive holes are used
16	0.093 $8 \times 8 \times 2$	80	BS	2SL 3CL	3.49–12.13	60°	41*	RT5880/Yes	Multilayer configuration
17	0.11 $14.5 \times 14.5 \times 1.6$	86.1	BS	1SL 2CL	2.3–15.8	45°	58	FR-4/No	Angular stability is poor
18	0.103 $10 \times 10 \times 1.6$	84	BS	1SL 2CL	3.1–13.3	45°	40*	FR-4/No	Larger footprint of the FSS
19	0.261 $11.53 \times 11.53 \times 0.508$	97	BS	1 SL 2CL	6.81–18.97	45°	61*	RO4003C/No	Low angular stability
21	0.18 $14 \times 14 \times 1.6$	94	BS	1SL 1CL	4–14	45°	59*	FR-4/No	Lower band is not covered
23	0.066 $8 \times 8 \times 1.6$	61	BS	1SL 1CL	2.72–13	40°	55*	FR-4/ No	Low angular stability
24	0.062 $6 \times 6 \times 1.6$	69.5	BS	1 SL 1CL	3.1–10.8	80°	45	FR-4/ No	Lack of conformability
28	0.074 $4 \times 4 \times 1.6$	69.3	BS	1 SL 1CL	2.8–17.1	60°	52*	FR-4/ No	Larger unit cell size
29	0.04 $12 \times 12 \times 0.8$	---	BS	1SL 2CL	1.01–9.84	45°	58*	FR-4/ No	Lack of angular stability
36	0.096 $7.6 \times 7.6 \times 0.168$	82.63	BP	3SL 3CL 2 F	3.79, 8.34, 12.52	50°	---	RO4350B	Large size of the FSS
37	0.148 $2.3 \times 2.3 \times 0.45$	92.32	BP	2SL 3CL	19.42, 42.78	60°	---	F4B	Bulkier profile
PW	0.041 $4 \times 4 \times 0.05$	–	BS	1SL 1CL	3.1–10.6	75°	67.9	Polyester/ Yes	–

Table 1. Performance comparison of the proposed FSS with similar existing designs. λ_0 : Wavelength at the lowest operating frequency, θ : Angular stability, *: Values obtained from the graph, OF operating frequency, SE shielding effectiveness, MF miniaturized footprint, %M percentage miniaturization, S substrate, C conformal, NOL number of layers, NOR nature of response, BP band-pass, BS band-stop, PW proposed work.

Data availability

The datasets used and/or analysed during the current study available from the corresponding author on reasonable request.

Received: 6 November 2024; Accepted: 27 February 2025

Published online: 05 April 2025

References

- Yue, S., Zeng, S., Liu, L., Eldar, Y. C. & Di, B. Hybrid Near-Far field channel Estimation for holographic MIMO communications. *IEEE Trans. Wireless Commun.* **23**(11), 15798–15813. <https://doi.org/10.1109/TWC.2024.3433491> (2024).
- Zhou, Y. J. et al. Smart meta-device powered by stray microwave energies: A green approach to shielding external interference and detection. *Appl. Energy.* **378**, 124770. <https://doi.org/10.1016/j.apenergy.2024.124770> (2025).
- Zhao, Y., Wang, X. & Huang, Z. Multi-Function radar modeling: A review. *IEEE Sens. J.* **24**(20), 31658–31680. <https://doi.org/10.1109/JSEN.2024.3436877> (2024).
- Huang, Z. et al. Joining Spatial deformable Convolution and a dense feature pyramid for surface defect detection. *IEEE Trans. Instrum. Meas.* **73**, 1–14. <https://doi.org/10.1109/TIM.2024.3370962> (2024).
- Fontana, R. J. Recent system applications of short-pulse ultra-wideband (UWB) technology. *IEEE Trans. Microw. Theory Tech.* **52**(9), 2087–2104 (2004).
- Revision of part 15 of the commission's rules regarding ultra-wideband transmission systems. Federal Commun. Commission, Washington, DC, USA, Tech. Rep. ET-Docket 98–153, FCC02-48. <https://doi.org/10.1016/j.aeue.2017.10.018> (2002).
- Bagci, F. et al. A glass based dual band frequency selective surface for protecting systems against WLAN signals. *AEU - Int. J. Electron. Commun.* **82**, 426–434. <https://doi.org/10.1016/j.aeue.2017.10.018> (2017).
- Zhang, X. et al. Target detection and positioning aided by reconfigurable surfaces: reflective or holographic?? *IEEE Trans. Wireless Commun.* **23**(12), 19215–19230. <https://doi.org/10.1109/TWC.2024.3480353> (2024).
- Kumar, A., Dwari, S. & Pandey, G. P. A dual-band high-gain microstrip antenna with a defective frequency selective surface for wireless applications. *J. Electromagn. Waves Appl.* **35**(12), 1637–1651. <https://doi.org/10.1080/09205071.2021.1914195> (2021).
- Hua, B., He, X. & Yang, Y. Polarisation-independent UWB frequency selective surface based on 2.5D miniaturised hexagonal ring. *Electron. Lett.* **53**, 1502–1504. <https://doi.org/10.1049/el.2017.2921> (2017).
- Khajevandi, A. & Oraizi, H. Miniaturization of frequency selective surface by 2.5-dimensional meandered split ring cells for application in L-band. *Sci. Rep.* **13**, 18737. <https://doi.org/10.1038/s41598-023-46159-z> (2023).
- Li, B. & Ne, R. A novel miniaturized dual-layer frequency selective surface. *AEU - Int. J. Electron. Commun.* **130**, 153580. <https://doi.org/10.1016/j.aeue.2020.153580> (2021).
- Hong, T., Guo, S., Jiang, W. & Gong, S. Highly selective frequency selective surface with ultrawideband rejection. *IEEE Trans. Antennas Propag.* **70**(5), 3459–3468. <https://doi.org/10.1109/TAP.2021.3137453> (2022).
- Hong, T., Wang, M., Peng, K., Zhao, Q. & Gong, S. Compact ultra-wide band frequency selective surface with high selectivity. *IEEE Trans. Antennas Propag.* **68**(7), 5724–5729. <https://doi.org/10.1109/TAP.2020.2963905> (2020).

15. Al-Sheikh, A. & Shen, Z. Design of wideband bandstop frequency-selective structures using stacked parallel strip line arrays. *IEEE Trans. Antennas Propag.* **64**(8), 3401–3409 (2016).
16. Hua, B. et al. Wide-angle frequency selective surface with ultra-wideband response for aircraft stealth designs. *Progress Electromagnet. Res. C* **77**, 167–173 (2017).
17. Shaik, V. & Inabathini, S. R. An ultra-wideband polarization insensitive frequency selective surface for shielding applications. *Int. J. RF Microw. Comput. Aided Eng.* **32**(4), e23065. <https://doi.org/10.1002/mmce.23065> (2022).
18. Sampath, S. S., Sivasamy, R. & Single-Layer, A. UWB frequency-selective surface with band-stop response. *IEEE Trans. Electromagn. Compat.* **62**(1), 276–279. <https://doi.org/10.1109/TEMC.2018.2886285> (2020).
19. Aziz, R. S. et al. Novel versatile topologies and design optimization of wide-bandstop frequency selective surfaces for X-band, Ku-band and millimeter-wave applications. *Sci. Rep.* **13**, 1952. <https://doi.org/10.1038/s41598-023-28922-4> (2023).
20. Coomar, S., Mondal, S. & Sanyal, R. Polarization-insensitive ultrathin fractal shaped frequency selective surface for ultra wide band shielding. *AEU - Int. J. Electron. Commun.* **147**, 154141. <https://doi.org/10.1016/j.aeue.2022.154141> (2022).
21. Sivasamy, R. et al. Polarization independent single layer ultrawideband frequency selective surface. *Int. J. Microwave Wirel. Technol.* **9**(1), 93–97. <https://doi.org/10.1017/S1759078715001439> (2015).
22. Sood, D. & Tripathi, C. C. Polarization insensitive compact wide Stop-band frequency selective surface. *J. Microwaves Optoelectron. Electromagn. Appl.* **17**, 53–64. <https://doi.org/10.1590/2179-10742018v17i11128> (2018).
23. Paul, G. S. & Mandal, K. Polarization-Insensitive and angularly stable compact ultrawide Stop-Band frequency selective surface, in IEEE antennas and wireless propagation letters. *Sept* **18**(9), 1917–1921 (2019).
24. Katoch, K., Jaglan, N. & Gupta, S. D. Design and analysis of single sided modified square loop UWB frequency selective surface. *IEEE Trans. Electromagn. Compatibil.* **63**(5), 1423–1432 (2021).
25. Prasad, P., Singh, S. N. & Kumar, A. A low profile RF shielding FSS with enhanced ultrawide bandwidth range and angular stability. *IntJRF Microw. Comput. Aided Eng.* **32**(9), e23261. <https://doi.org/10.1002/mmce.23261> (2022).
26. Sivasamy, R. & Kanagasabai, M. Novel reconfigurable 3-D frequency selective surface. *IEEE Trans. Compon. Packag. Manuf. Technol.* **7**(10), 1678–1682. <https://doi.org/10.1109/TCMPMT.2017.2688367> (2017).
27. Sivasamy, R. & Kanagasabai, M. Design and fabrication of flexible FSS polarizer. *Int. J. RF Microw. Comput. Aided Eng.* **30**, e22002. <https://doi.org/10.1002/mmce> (2020).
28. Mandal, G. S. P. K. & Ali Lalbakhsh Single-layer ultra-wide stop-band frequency selective surface using interconnected square rings. *AEU - Int. J. Electron. Commun.* **132**, 153630. <https://doi.org/10.1016/j.aeue.2021.153630> (2021).
29. Mellita, R. A., Chandu, D. S., Karthikeyan, S. S. & Damodharan, P. A miniaturized wideband frequency selective surface with interconnected cell structure. *AEU-International J. Electron. Commun.* **120**, 1–7. <https://doi.org/10.1016/j.aeue.2020.153196> (2020).
30. Thakare, R., Kulat, K. D., Santosh, C. & Overview and analysis of UWB signal for low power WPAN. *Int. J. Comput. Appl.* **1**, 70–659. 10.5120/ (2010).
31. Durantini, A. & Mazzenga, F. UWB Interference mitigation techniques in a cooperative scenario. in *The 18th Annual IEEE International Symposium on Personal, Indoor and Mobile Radio Communications (PIMRC'07)*.
32. Khajevandi, A. & Oraizi, H. Utilizing interdigital and supershape geometries for the design of frequency selective surfaces with high angular and polarization stabilities. *Sci. Rep.* **12**, 7054. <https://doi.org/10.1038/s41598-022-10960-z> (2022).
33. Daira, S. E. I. et al. A curved single-layer FSS design for gain improvement of a compact size CPW-fed UWB monopole antenna. *Microw. Opt. Technol. Lett.* **66**, e33943. <https://doi.org/10.1002/mop.33943> (2024).
34. Kanagasabai, M. et al. A novel ultra-miniaturized angularly stable frequency selective surface for L-Band shielding applications. *Int. J. Antennas Propag.* <https://doi.org/10.1155/2024/8777541>
35. Ramprabhu Sivasamy, M. et al. A novel shield for GSM 1800 mhz band using frequency selective surface. *Progress Electromagnet. Res. Lett.* **38**, 193–199. <https://doi.org/10.2528/PIERL13022206> (2013).
36. Li, Z. et al. Design and analysis of a complementary structure-based high selectivity tri-band frequency selective surface. *Sci. Rep.* **14**, 9415. <https://doi.org/10.1038/s41598-024-59712-1> (2024).
37. Li, Z. et al. A broadband second-order bandpass frequency selective surface for microwave and millimeter wave application. *Sci. Rep.* **14**, 12040. <https://doi.org/10.1038/s41598-024-62228-3> (2024).
38. Baisakhiya, S., Sivasamy, R., Kanagasabai, M. & Periaswamy, S. Novel compact UWB frequency selective surface for angular and polarization independent operation. *Progress Electromagn. Res. Lett.* **40**, 71–79. <https://doi.org/10.2528/PIERL13022707> (2013).
39. Hongyun, C., Mengyao, Y., Xue, P. & Ge, X. Joint active and passive beamforming design for hybrid RIS-Aided integrated sensing and communication. *China Commun.* **21**(10), 1–12. <https://doi.org/10.23919/JCC.ja.2023-0213> (2024).
40. Wu, Z. & Ismail, M. Generalized RIS tile exclusion strategy for indoor MmWave channels under concept drift. *IEEE Trans. Wireless Commun.* **23**(10), 13484–13498. <https://doi.org/10.1109/TWC.2024.3402267> (2024).
41. Chu, H., Pan, X., Jiang, J., Li, X. & Zheng, L. Adaptive and robust channel Estimation for IRS-Aided Millimeter-Wave communications. *IEEE Trans. Veh. Technol.* **73**(7), 9411–9423. <https://doi.org/10.1109/TVT.2024.3385776> (2024).
42. Guan, Y. et al. Regulable crack patterns for the fabrication of high-performance transparent EMI shielding windows. *iScience* **28**(1), 111543. <https://doi.org/10.1016/j.isci.2024.111543> (2025).
43. Zhang, L. et al. Design of Temperature-Pressure sensor based on Slot-Antenna CSRR integrated for applications in High-Temperature environments. *IEEE Sens. J.* **24**(17), 27218–27224. <https://doi.org/10.1109/JSEN.2024.3423023> (2024).
44. Dai, M., Sun, G., Yu, H., Wang, S. & Niyato, D. User association and channel allocation in 5G mobile asymmetric Multi-Band heterogeneous networks. *IEEE Trans. Mob. Comput.* <https://doi.org/10.1109/TMC.2024.3503632> (2024).
45. Govindan, T. et al. Design and analysis of a flexible smart apparel MIMO antenna for bio-healthcare applications. *Micromachines* **13**(11), 1919. <https://doi.org/10.3390/mi13111919> (2022).

Acknowledgements

This research was supported in part by the National Research and Development Program through the National Research Foundation of Korea (NRF) funded by the Ministry of Science and ICT (No. RS-2023-00281275), and in part by the BK21 FOUR project funded by the Ministry of Education (No. 4199990113966).

Author contributions

M.K., L.V. and M.G.N.A. conceived and performed simulations, experiment, and drafted the manuscript. S.K.P., S.K. and S.P.P. conducted the experiment. H.C.C. and K.W.K. analyzed the results. S.K. and K.W.K. supervised the overall work and provided funding for the experiments. All authors reviewed the manuscript.

Declarations

Competing interests

The authors declare no competing interests.

Additional information

Correspondence and requests for materials should be addressed to S.K.P. or K.W.K.

Reprints and permissions information is available at www.nature.com/reprints.

Publisher's note Springer Nature remains neutral with regard to jurisdictional claims in published maps and institutional affiliations.

Open Access This article is licensed under a Creative Commons Attribution-NonCommercial-NoDerivatives 4.0 International License, which permits any non-commercial use, sharing, distribution and reproduction in any medium or format, as long as you give appropriate credit to the original author(s) and the source, provide a link to the Creative Commons licence, and indicate if you modified the licensed material. You do not have permission under this licence to share adapted material derived from this article or parts of it. The images or other third party material in this article are included in the article's Creative Commons licence, unless indicated otherwise in a credit line to the material. If material is not included in the article's Creative Commons licence and your intended use is not permitted by statutory regulation or exceeds the permitted use, you will need to obtain permission directly from the copyright holder. To view a copy of this licence, visit <http://creativecommons.org/licenses/by-nc-nd/4.0/>.

© The Author(s) 2025